EGF induces microRNAs that target suppressors of cell migration: miR-15b targets MTSS1 in breast cancer

Growth factors and their receptors play critical roles in tumor progression, by acting as mitogens, mediators of cell migration, and enhancers of drug resistance (*1*, *2*). For example, the epidermal growth factor (EGF) induces biochemical and morphological changes in its target cells, which result in a myriad of cellular outcomes, including proliferation and migration of glial and epithelial cells (*3*, *4*). These morphological and behavioral changes can be pathogenic and lead to the development and progression of cancer. Often, EGF-inducible genes, such as *CTEN*, which encodes an integrin-binding protein, are overexpressed in aggressive mammary tumors (*3*, *5*), whereas the expression of genes encoding proteins that normally suppress EGF signaling is decreased (*6*). These associations between pathological and tran-scriptional attributes of tumors might extend to noncoding RNAs. We previ-ously showed that EGF induced a rapid decrease in the expression of a group of microRNAs (miRNAs) that we called "immediate down-regulated" miRNAs (ID-miRs). These miRNAs are frequently decreased in tumors and target a group of mRNAs corresponding to oncogenic genes that are induced quick-ly upon EGF stimulation ("immediate early" genes), such as *FOS* and *JUN* (*7*). Likewise, cell transformation or motility may be enabled if growth factor signaling induces a set of miRNAs that target tumor suppressors. Thus, growth factor–inducible changes in the levels of coding and noncoding RNAs create a homeostatic feedback regulatory system, which is often defective in cancer (*6*, *8*).

It is unclear what role many miRNAs have in regard to tumorigenesis. For example, miR-15b is overexpressed in various tumors, including melanomas and lesions in the liver, colon, and cervix (*9*–*12*). By contrast, analyses of glioma cell lines raised the possibility that miR-15b arrests the cell cycle by suppressing the abundance of cyclin E1 (*13*). MTSS1 [also known as MIM (missing in metastasis)] is a scaffold protein containing multiple domains, including a WASP (Wiskott-Aldrich syndrome protein) homology 2 (WH2) domain and an inverse Bin-Amphiphysin-Rvs (I-BAR) domain. *MTSS1* mRNA is decreased in metastatic cell lines of bladder and prostate tumors (*14*). In tumors from gastric and breast cancer patients, the abundance of MTSS1 was lower in progressed disease stages (*15*, *16*).

MTSS1 abundance is regulated by both DNA methylation and miRNAs. Regulation of MTSS1 abundance by three miRNAs—miR-182, miR-23a, and miR-135a—was demonstrated in ovarian, prostate, hepatocellular, and colorectal cancer cells (*17*–*22*). MTSS1 binds actin and phosphatidylinositol 4,5-bisphosphate (PIP_2)–rich membranes, thereby linking the cytoskeleton to the plasma membrane (*23*). MTSS1 is also required for the maintenance of cell-cell junctions in mouse epithelial kidney cells and in human head and neck cancer cells (*24*, *25*). Here, we investigated the link between EGF-inducible miRNAs and breast cancer progression, specifically the functional interaction between miR-15b and MTSS1 in cell locomotion.

In line with previous reports (*26*, *27*), stimulation of human MCF10A mammary epithelial cells with EGF induced rapid remodeling of the actin cytoskeleton,

[1]Department of Biological Regulation, Weizmann Institute of Science, Rehovot 76100, Israel. [2]Division of Molecular Genome Analysis, German Cancer Research Center (DKFZ), Heidelberg 69120, Germany. [3]Department of Physics of Complex Systems, Weizmann Institute of Science, Rehovot 76100, Israel. [4]Translational Oncogenomics Unit, Italian National Cancer Institute "Regina Elena," Rome 00144, Italy. [5]Laboratory Medicine and Pathobiology, Faculty of Medicine, University of Toronto and Department of Pathology, University Health Network, Toronto, Ontario M5C 2C4, Canada. [6]IPATIMUP, University of Porto, Porto 4200–465, Portugal.
*Present address: Genetic Institute, Tel Aviv Medical Centre, Tel Aviv 64239, Israel.
†Present address: Unit of Histology, Embryology and Applied Biology, Department of Experimental, Diagnostic and Specialty Medicine, University of Bologna, Bologna 40126, Italy.
‡Present address: Center for Genomic Science of IIT@SEMM, Fondazione Istituto Italiano di Tecnologia (IIT), Via Adamello 16, 20139 Milan, Italy.
§Corresponding author. E-mail: yosef.yarden@weizmann.ac.il

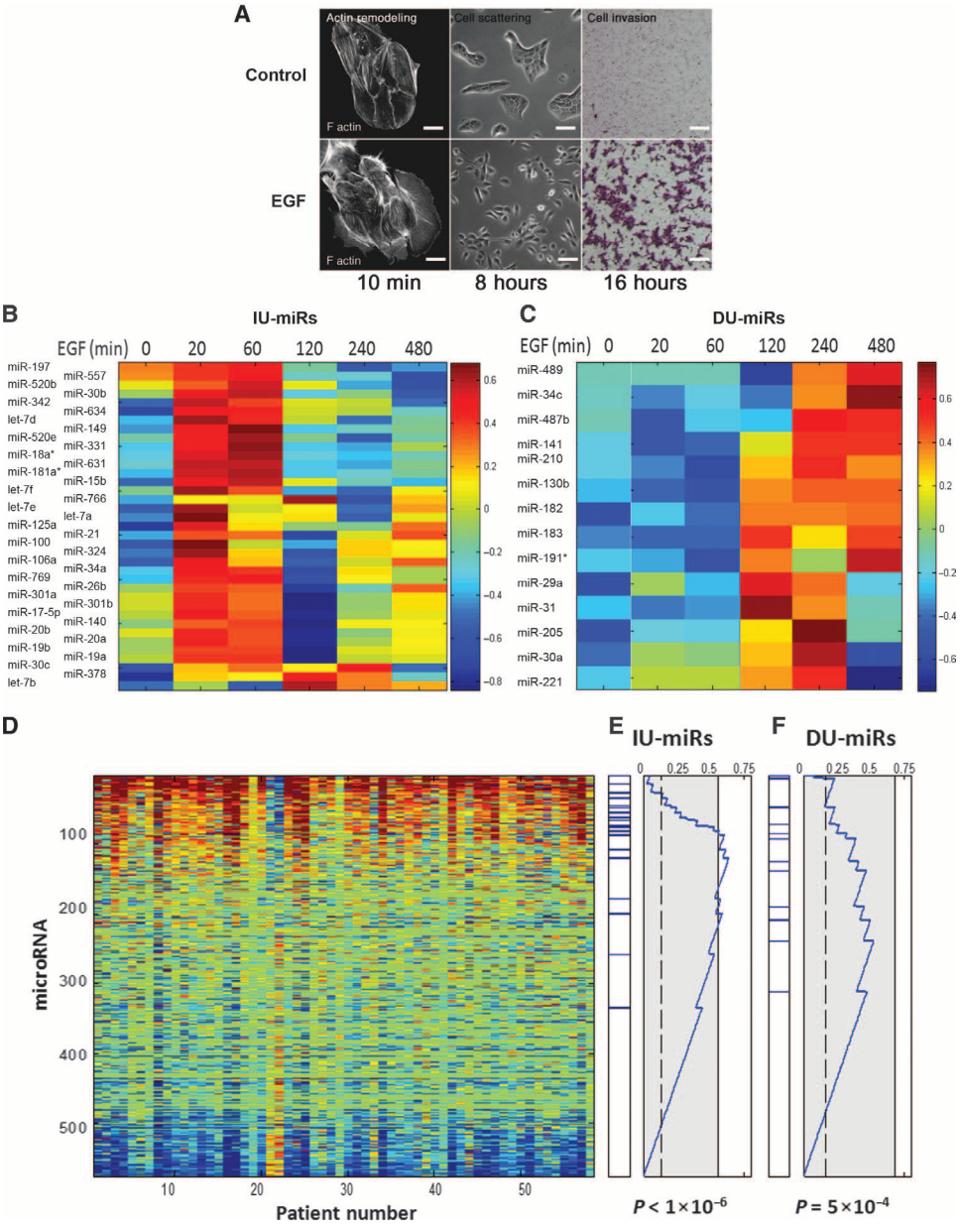

Fig. 1. A set of EGF-induced miRNAs is significantly enriched in mammary tumors compared to surrounding tissue. (**A**) Actin (left), cell scattering (middle), and cell migration (right) in MCF10A cells stimulated with EGF (10 ng/ml) for the indicated time. Scale bars, 20, 50, and 250 μm, respectively. (**B** and **C**) Results of oligonucleotide miRNA arrays extracted from previously published data (*7*), in which MCF10A cells were incubated with EGF (10 ng/ml) for the indicated time. The inducible miRNAs were divided into two groups: IU-miRs (B) and DU-miRs (C). (**D**) Heatmap of the fold change of miRNAs in the tumor tissue compared to matched surrounding nontumor tissue, analyzed in a breast cancer patient data set (*28*), in which the expression of about 550 miRNAs in pairs of a tumor and the adjacent tissue (from 58 patients). miRNAs were sorted according to a combined *P* value of the average relative change. (**E** and **F**) Enrichment of immediate (E) or delayed (F) EGF-induced miRNAs in mammary tumors. For each panel, the blue horizontals in the left column mark where individual IU-miRs and DU-miRs correspond to on the heatmap in (D). The graphs in the right columns show the enrichment curves and *P* values. The enrichment scores, in comparison to random permutations (gray area), were 0.63 for IU-miRs and 0.52 for DU-miRs. The dashed vertical lines indicate mean enrichment score of randomly selected groups of miRNAs.

colony scattering, and matrix invasion (Fig. 1A). These changes might be governed by newly synthesized mRNAs and miRNAs. We previously characterized the dynamic changes in the abundance of miRNAs in EGF-treated MCF10A cells by means of profiling miRNA expression using DNA arrays (*7*). Reanalysis of these results defined a group of 37 miRNAs that had >1.5-fold increased abundance within 60 min of EGF stimulation (Fig. 1B); herein, we refer to these as "immediate up-regulated" miRNAs (IU-miRs). Additionally, 14 miRNAs, the abundance of which was increased at later time points, were identified (Fig. 1C), and we have classified these as "delayed up-regulated" miRNAs (DU-miRs) (Fig. 1C). Quantitative reverse transcription polymerase chain reaction (qRT-PCR) validated the induction of 22 IU-miRs within 60 min and enabled further division of this group into three sets according to their onset times (fig. S1). Because the abundance of miRNAs that were suppressed upon stimulation with EGF can differentiate between malignant and normal breast tissues (*7*), we analyzed all inducible miRNAs in a data set that compared miRNA abundance in tumors against that in the surrounding normal tissues (peritumor) (*28*) (Fig. 1D). As expected, IU-miRs showed statistically significant enrichment among miRNAs that had a higher abundance in tumors compared to the matched peritumor tissue (Fig. 1E). Similarly, the DU-miRs were also enriched in the group of miRNAs that were increased in tumors (Fig. 1F), implying that processes occurring in advanced mammary tumors are mirrored by mammary cells stimulated with a growth factor in culture.

MiRNA profiles can be classified according to molecular subtypes of breast cancer (*29*–*31*). To investigate whether the EGF-induced miRNAs we identified are associated with specific breast cancer subtypes, we analyzed the data set by Enerly *et al.* (*29*), which profiled miRNAs in samples from 101 breast cancer patients. We found that 8 of the verified 22 IU-miRs were significantly associated with the luminal A subtype, whereas 6 other IU-miRs were significantly associated with the basal subtype (Fig. 2A and table S1). Among the DU-miRs, only a few miRNAs were significantly associated with specific subtypes (Fig. 2B). These observations, along with the lower clinical significance of DU-miRs, as compared to IU-miRs (Fig. 1F), suggest

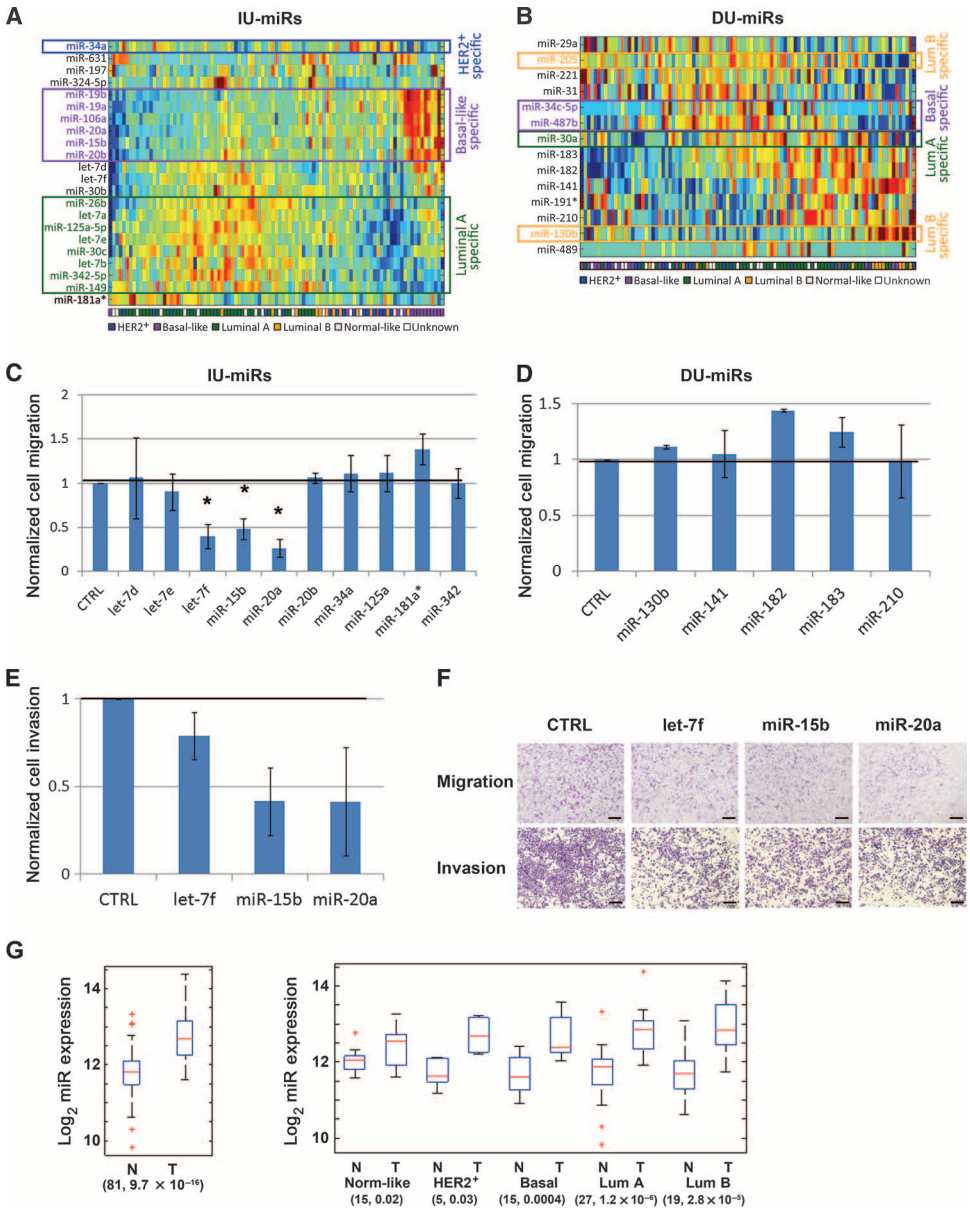

Fig. 2. Association of IU-miRs with breast cancer subtypes and with cellular motility. (**A** and **B**) SPIN-ordered (see Materials and Methods) expression matrices of the validated 22 IU-miRs (A) and 14 DU-miRs (B) in a set of 101 primary breast tumors obtained from Gene Expression Omnibus (GEO) series GSE19536 (*29*). Red, relatively high abundance; blue, relatively low abundance. n = 16 HER2-positive (HER2$^+$), 15 basal-like, 41 luminal A (Lum A), 12 luminal B, and 10 normal-like patients, along with 6 tumors of unknown subtype, corresponding to the color-coded legend along the bottom. Analysis of variance (ANOVA) and false discovery rate–corrected P values ($P < 0.05$) were used. (**C** and **D**) Transwell migration in EGF-treated MCF10A cells, in which each of the top 10 IU-miRs (C; *$P < 0.001$, one-way ANOVA) and the top 5 DU-miRs (D) from Fig. 1 (B and C) were knocked down with anti-miRs, normalized to cells transfected with control small interfering RNA (siRNA). Data are representative of three experiments. Relative induction of IU-miRs let-7f, miR-15b, and miR-20a was significant ($P < 0.001$, one-way ANOVA). (**E**) Matrigel invasion by MDA-MB-231 cells transfected either with a control siRNA or with the indicated anti-miR. Data are relative means ± SD from three experiments ($P < 0.001$, one-way ANOVA). (**F**) Crystal violet staining micrographs of migration and invasion by MCF10A and MDA-MB-231 cells, respectively, transfected with the indicated anti-miRs or with a control siRNA (CTRL). Images are representative of three experiments. Scale bars, 200 μm. (**G**) Abundance of miR-15b in tumors (T) and normal (N) tissues corresponding to a published breast cancer patient data set (*31*). Left, whole data set; right, divided by subtype. Boxes represent the distribution of abundance. Numbers in brackets below the graphs refer to the number of analyzed patients and the respective P values.

that the observed onset times of specific miRNAs in cultured cells might be relevant to disease parameters.

Because EGF induced robust cell migration in our culture model, we next addressed the roles for the inducible miRNAs in motility. For this, we selected 10 IU-miRs and 5 DU-miRs that showed highest differences in breast cancer, relative to the surrounding noncancerous tissue. Each miRNA was knocked down using anti-miR inhibitors in MCF10A cells, and the migration capacities of the respective cells were tested using Transwell assays (Fig. 2, C and D). Of the 15 miRNAs we tested, let-7e, miR-20a, and miR-20b were included in our previous analysis of cell migration (*32*). Three of the 10 selected IU-miRs significantly decreased cell migration when silenced (Fig. 2C), whereas knocking down 2 of the 5 DU-miRs only moderately stimulated cell migration (Fig. 2D). Additionally, knocking down the three IU-miRs that affected migration, namely, let-7f, miR-15b, and miR-20a, also reduced the invasion capacity of the highly invasive MDA-MB-231 breast cancer cells (Fig. 2, E and F). These results suggest that specific IU-miRs promote migration, whereas some of the DU-miRs, induced later, might repress migration. To examine this scenario, we transfected MCF10A cells with mimic versions of a group of DU-miRs. Almost all DU-miRs that we tested inhibited migration (fig. S2, A and B), in agreement with a late, miRNA-mediated inhibitory switch that arrests cell migration.

To investigate the potential clinical implications of the three active IU-miRs, we compared their abundance in mammary tumors and in matched normal tissues from a published data set (*31*). MiR-15b was the only miRNA out of the three that had a significantly higher abundance in the tumors than the normal tissues in all five breast cancer subtypes (Fig. 2G). These observations led us to focus the rest of the study on the three migration-promoting IU-miRs, especially miR-15b.

To predict mRNA targets of the three migration-promoting miRNAs (let-7f, miR-15b, and miR-20a), we used miRecords (*33*), which integrates 11 different prediction tools. Only targets that were predicted by at least five of the tools were considered, resulting in 350 to 550 predicted genes for each miRNA. To identify more relevant transcripts to the conditions of interest, we compared the list of predicted targets to the list of transcripts that were sup-pressed in MCF10A cells upon stimulation with EGF (*6*). We identified only a single putative target of let-7f, which encoded a member of the ZNF family, but several suitable targets of the other two IU-miRs (Fig. 3A). Because we had observed that the abundance of miR-15b was significantly higher in mammary tumors compared to normal tissue (Fig. 2G), but the trend for miR-20a was less clear, we selected miR-15b for further investigation. We used PCR and validated that 9 of the 11 putative targets of miR-15b decreased over extended time upon EGF stimulation (Fig. 3B). To identify targets that control cell migration, we assessed the effect of knocking down each of those nine mRNAs on EGF-induced migration.

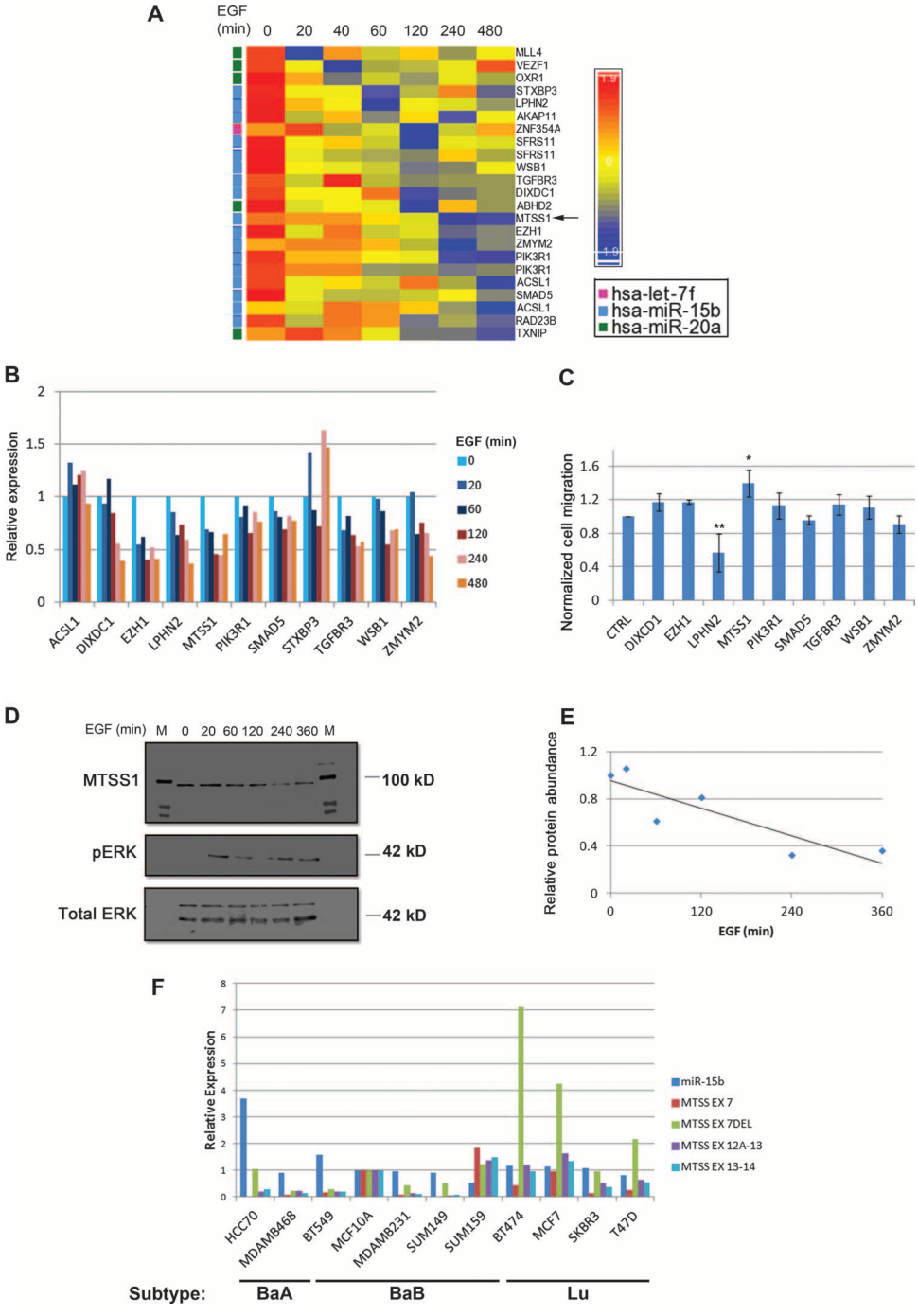

Fig. 3. Several putative targets of miR-15b regulate cell migration. (**A**) miRecords (*33*)–predicted targets of miR-15b. Listed are transcripts that were predicted by at least five different computational tools, denoted by the color-coded legend down the left side of the heatmap. The dynamics of their decrease (color scale, right) are shown according to previously published data (*6*). (**B**) qRT-PCR analysis of the indicated miR-15b target mRNAs in MCF10A cells stimulated with EGF (10 ng/ml) for up to 8 hours. Data are representative of two experiments. (**C**) Transwell migration results obtained with MCF10A cells pretransfected with siRNAs against each of the nine predicted miR-15b targets and presented relative to migration exhibited by cells transfected with a control siRNA upon stimulation with EGF (10 ng/ml). Data are means ± SD from three experiments (**P* = 0.01, ***P* = 0.002). (**D** and **E**) Western blotting (D) and quantification (E) for MTSS1 and phosphorylated (p) or total ERK of MCF10A cells stimulated for the indicated time intervals with EGF (10 ng/ml). Data are representative of two experiments. (**F**) qRT-PCR for the abundance of alternatively spliced forms of *MTSS1* mRNAs in a panel of human mammary tumor cell lines. BaA and BaB, basal type A and type B, respectively; Lu, luminal. Data are representative of two experiments.

These assays identified two migration-regulating genes: *LPHN2* [encoding latrophilin 2, a G protein (heterotrimeric guanine nucleotide–binding protein)–coupled receptor located in loci that show high frequency of loss of heterozygosity in human breast cancers (*34*)] reduced cell migration when knocked down, whereas *MTSS1* (described above) enhanced cell migration when silenced (Fig. 3C). On the basis of these results, we selected *MTSS1*, a presumed target of miR-15b, for further investigation. The abundance of MTSS1 at both the mRNA and protein levels was decreased upon EGF stimulation of MCF10A cells (Fig. 3, D and E). Together, these results suggest that EGF-induced miR-15b suppresses the translation or abundance of the transcript encoding MTSS1, and the loss of MTSS1 promotes migration of mammary cells.

MTSS1 [also called missing in metastasis (MIM-A)] has been characterized as an actin-binding scaffold that has several functional domains, including a BAR-like domain, which can interact with membranes to induce membrane deformation, and also with actin and the small guanosine triphosphatase (GTPase) Rac (*35*). Several *MTSS1* alternative splicing transcripts have been identified, including a 12–base pair deletion at the 5′ junction of exon 7 and an alternative exon 12 (fig. S3A). Moreover, Loberg and colleagues showed that the abundance of several variants is reduced in human prostate cancers (*36*). Similarly, we detected four isoforms of MTSS1 in breast cancer cell lines, but the abundance of each greatly differed (Fig. 3F). For example, an isoform missing exon 7 appears to be enriched in luminal cell lines, whereas a variant in exon 12 is mostly absent in cell lines derived from basal tumors. The functional implications of each variant are an area for future investigation.

miR-15b regulates the abundance of MTSS1

To examine the prediction that *MTSS1* serves as a novel target of miR-15b, we undertook several approaches. First, we evaluated the expected temporal correlation between *MTSS1* mRNA abundance and that of miR-15b in EGF-stimulated cells, which confirmed a predicted negative correlation in MCF10A cells (Fig. 4A). Second, by using a data set that surveyed both mRNA and miRNA in individual breast cancer patients (*29*), we compared the abundance of *MTSS1* mRNA and miR-15b in different molecular subtypes. This comparison found that the amount of miR-15b was highest in the basal-like subtype, a disease often driven by growth factor signaling, and correspondingly, the abundance of *MTSS1* mRNA was significantly lower in this subtype (Fig. 4B). Third, the abundance of *MTSS1* was analyzed at both mRNA and protein levels in cells that were pretransfected with either a mimic or an inhibitor of miR-15b in the presence of EGF. As expected, *MTSS1* transcript and protein amounts were lower in mimic-15b–transfected cells than in control cells, and higher in the cells pretransfected with the miR-15b inhibitor (Fig. 4, C and D). Finally, to ascertain that miR-15b directly regulates *MTSS1*, we used a luciferase reporter construct containing the 3′ untranslated region (3′UTR) sequence of *MTSS1* and mutated the site corresponding to the predicted miR-15b seed sequence (Fig. 4E). Three bases were mutated while preserving the GC content of this segment. As expected, the wild-type MTSS1-3′UTR cotransfected with anti–miR-15b produced significantly higher luminescence signals than did the

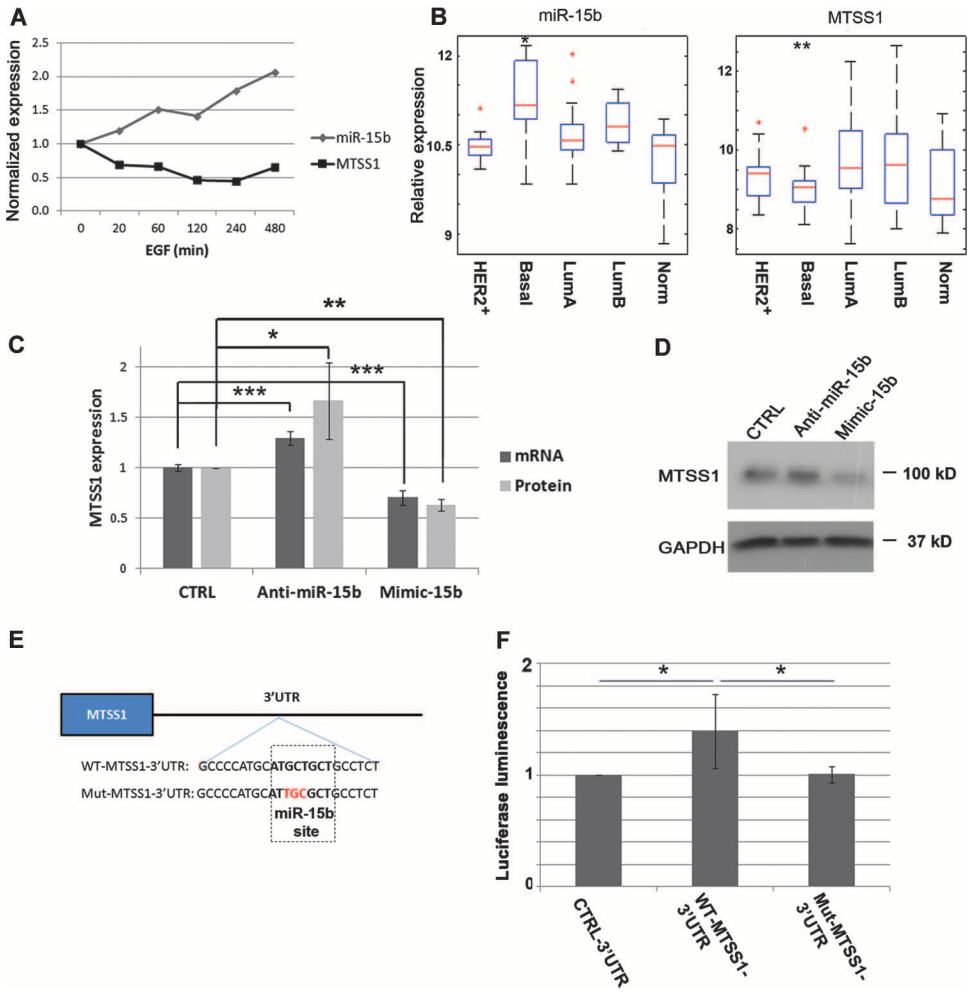

Fig. 4. miR-15b suppresses MTSS1 abundance. (**A**) qRT-PCR for miR-15b and *MTSS1* mRNA in MCF10A cells stimulated with EGF (10 ng/ml) for the indicated time. Data are representative of two experiments. $R = -0.59$ by Pearson correlation. (**B**) Abundance of miRNA-15b (left) and *MTSS1* mRNA (right) in human breast cancer samples of various subtypes: HER2$^+$ (HER2-positive, $n = 16$), Basal ($n = 15$), LumA (luminal A, $n = 41$), LumB (luminal B, $n = 12$), and Norm (normal-like, $n = 10$). $^*P = 5.81 \times 10^{-5}$, $^{**}P = 0.0124$, one-way ANOVA. (**C** and **D**) qRT-PCR and Western blotting probing for MTSS1 mRNA and protein in MCF10A cells that were pretransfected with a miR-15b mimic, an anti–miR-15b, or a control plasmid. Data are means ± SD from three experiments ($^*P = 0.09$, $^{**}P < 0.01$, $^{***}P < 0.005$). (**E**) Schematic and nucleotide sequence of the 3′UTR of *MTSS1*, specifically the putative binding site of miRNA-15b. Red residues indicate the mutation created within this sequence. (**F**) Luminescence of HeLa cells cotransfected with either an anti–miRNA-15b or a control siRNA, along with a luciferase reporter containing the wild-type (WT) or mutant (Mut) form of the *MTSS1* 3′UTR construct or a control plasmid. Data are means ± SD from five experiments; $P < 0.05$, one-way ANOVA, followed by Bonferroni correction.

control plasmid (Fig. 4F). In addition, when a mutation in the single predicted binding site of miR-15b was introduced into the MTSS1-3′UTR reporter, the luminescence signal was similar to the control and significantly lower than the signal obtained with the wild-type 3′UTR (Fig. 4F). In aggregate, our results identified *MTSS1* as an in vitro target of miR-15b and provided evidence suggesting that these relationships extend to human mammary tumors.

To phenocopy the IU-miR–induced repression of *MTSS1*, we applied the respective short hairpin RNA (shRNAs) on both normal and breast cancer cell lines. Our qRT-PCR analyses, which tested several different shRNAs, verified decreases of the wild-type and alternative transcripts of MTSS1 in mam-mary cells (fig. S3, B to F), and immuno-blotting confirmed that the respective protein was also decreased (Fig. 5A). In addition, we made use of an expression vector containing the coding region of *MTSS1* but lacking the 3′ UTR. Because the binding site of miR-15b was deleted, this truncated version of MTSS1 was no longer under control of miR-15b. Then, we transfected mimic–miR-15b into mammary cells that ectopically overexpress the truncated sequence of *MTSS1* (fig. S3G). When mimic–miR-15b was transfected into control cells, their migration capacity slightly increased, probably due to suppression of the endogenous form of MTSS1. In line with the suppressive activity of MTSS1, when ectopically introduced, it weakly inhibited cell migration. Under these conditions, mimic-15b induced no increase in migration, in line with the inability of miR-15b to regulate the truncated form of MTSS1. Notably, MTSS1 acts as an inhibitor of cell motility when ectopically expressed in NIH3T3 fibroblasts (*37*), MDA-MB-435 mammary cells (*16*), PC-3 lung cancer cells and DU145 prostate cancer cells (*17*). In agreement with these observations, knocking down MTSS1 in several mammary cell lines promoted migration and invasion compared to control cells (Fig. 5, B and C). Reciprocally, ectopic stable ex-pression of a fusion protein constituting MTSS1 and the green fluorescent protein (GFP) retarded both migration and invasion of the highly metastatic MDA-MB-231 cell line (Fig. 5, D to F). Similarly, extension of gain- and loss-of-function analyses of MTSS1 and miR-15b to two basal breast

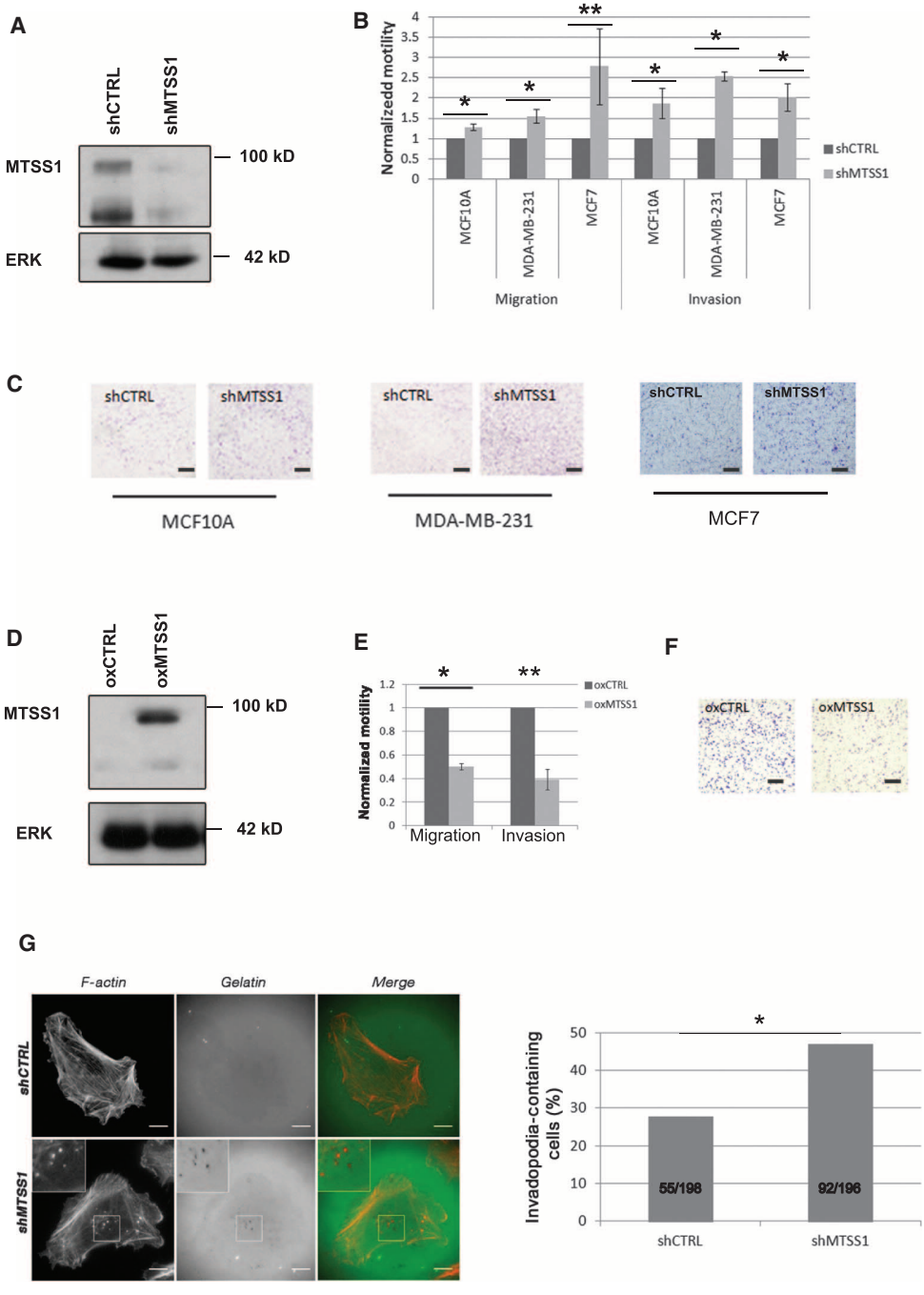

Fig. 5. MTSS1 decreases cell motility and the formation of invadopodia. (**A**) Western blotting to confirm MTSS1 knockdown in MCF10A cells. (**B** and **C**) Migration and Matrigel invasion exhibited by cells infected with MTSS1-shRNA relative to cells expressing control shRNA. (C) Images of migration. Data are means ± SD from three experiments. **P* < 0.05, ***P* = 0.08, *t* test. Scale bars, 200 μm. (**D** to **F**) MDA-MB-231 cells over-expressing MTSS1 were analyzed as in (A) to (C) relative to cells expressing a control plasmid. Data are means ± SD from three experiments. **P* = 0.02, ***P* = 0.007, *t* test. (**G**) Invadopodia formation in MTSS1-depleted and control MDA-MB-231 cells seeded on FITC (fluorescein isothiocyanate)–gelatin (green) and stained for actin using rhodamine phalloidin (red). Data are the sum of three independent experiments. **P* = 0.0001, χ^2 test. Inset, enlarged to show colocalization of actin and degraded gelatin in invadopodia. Scale bars, 10 μm.

tumor lines, SUM159 and BT549, confirmed reciprocal effects on cell migration (fig. S4, A to C).

Because invasion of cells through the extracellular matrix often involves formation of actin-filled, proteolytically active protrusions called invadopodia (*38*), we functionally analyzed these organelles by plating cells on a layer of fluorescent gelatin and quantifying fluorescence-free holes. Using this method, we found that silencing MTSS1 was associated with an increased fraction of cells exhibiting invadopodial structures (Fig. 5G and fig. S3E). Notably, previous studies linked invadopodia formation to an intracellular switch involving Src, cortactin, and growth factors (*39*), and MTSS1 appears to antagonize Src-dependent phosphorylation of cortactin (*40*). Hence, it is possible that the miR-15b–mediated decrease of MTSS1 upon EGF stimulation stabilizes invadopodia by means of the Src-cortactin switch.

MTSS1 interacts with actin monomers through its WH2 domain (*41*), and endogenous MTSS1 has been shown to accumulate on a subset of actin stress fibers (*42*). Consistent with these observations and a previous study that analyzed C3H10T1/2 cells (*42*), ectopic expression of GFP-MTSS1 significantly reduced the number of actin stress fibers in MDA-MB-231 cells (Fig. 6, A and B). Accordingly, the number of actin stress fibers increased in MCF7 cells that were stably depleted of endogenous MTSS1 (Fig. 6, C and D).

The involvement of MTSS1 in the formation and maintenance of intercellular junctions is another function of MTSS1, which suggests that it might regulate migration (*24*, *25*). The highly motile triple-negative breast cancer cell line we used, MDA-MB-231, hardly forms intercellular contacts. However, when we overexpressed MTSS1, MDA-MB-231 cells formed significantly more cell-cell junctions relative to control cells (Fig. 6, E and F). The endogenous abundance of MTSS1 in MDA-MB-231 cells is quite low (Fig. 5D). Thus, our findings are consistent with previously published data, which demonstrated that MTSS1 contributes to the integrity of cell-cell contacts in kidney epithelia (*25*), as well as enhances junctional strength in head and neck squamous carcinoma cells (*24*). In conclusion, these data suggest that MTSS1 has critical roles in restricting cell motility, probably by means of its involvement in the regulation of the actin cytoskeleton and intercellular junctions.

To decipher if MTSS1 can control mammary cell growth in addition to motility, we used both in vitro and in vivo approaches. When seeded in extracellular matrix, MTSS1-depleted MCF10A cells formed smaller spheroids than those formed by control cells (Fig. 7A). Despite their smaller sizes, MTSS1-depleted spheroids more frequently breached their laminin 5–enriched basement membrane than did controls. To examine the prediction that the smaller spheroids reflected slower proliferation, we performed BrdU (5-bromo-2′-deoxyuridine) incorporation assays in two-dimensional (2D) monolayers. When grown without EGF, the extent of BrdU incorporation into DNA was relatively low in both cell derivatives. Nevertheless, BrdU incorporation was increased in the presence of EGF in control cells but not in MTSS1-depleted cells (Fig. 7B). Together, these results demonstrated

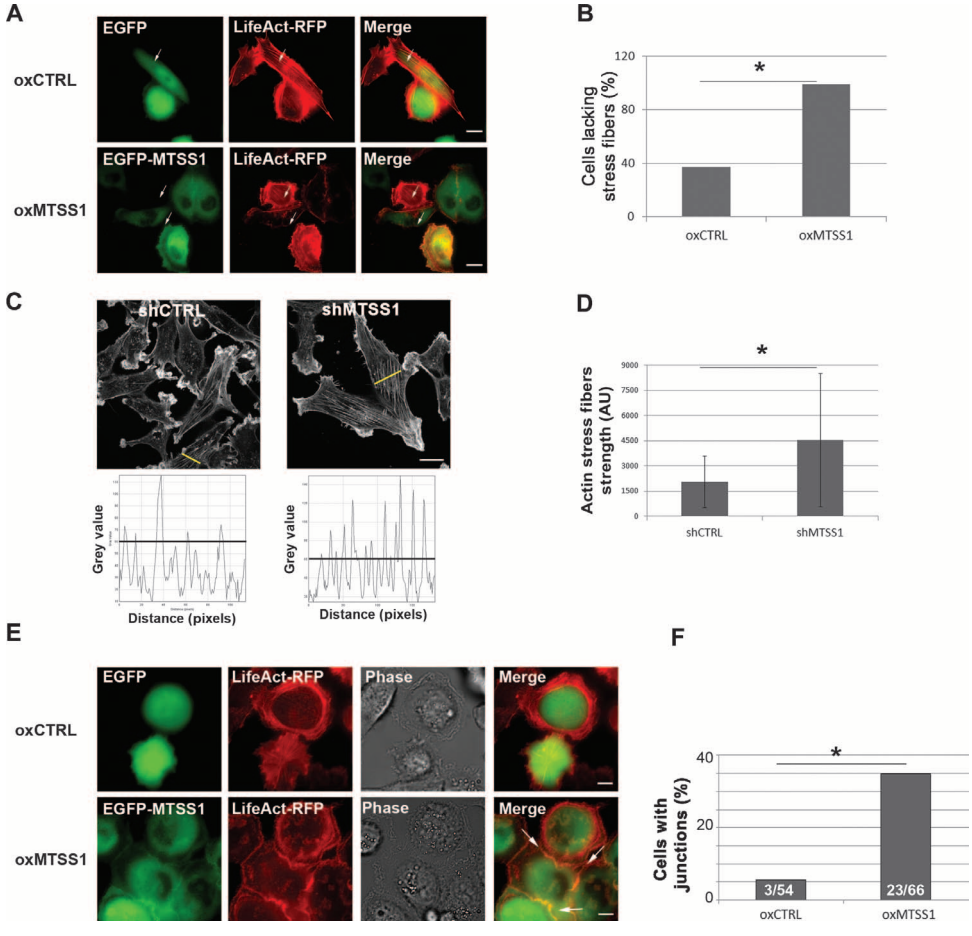

Fig. 6. MTSS1 inhibits the formation of actin stress fibers and enhances the formation of intercellular junctions. (**A** and **B**) Actin staining (A, red) and the number of cells lacking actin stress fibers (B) in MDA-MB-231 cells stably coexpressing EGFP or EGFP-MTSS1 and LifeAct-RFP plated on fibronectin-coated slides. Data are representative of two experiments from which 68 and 91 cells were analyzed in control and in MTSS1-overexpressing (ox) cells, respectively. **P* < 0.0001, χ^2 test. Scale bars, 20 μm. (**C** and **D**) MTSS1-depleted and control MCF7 cells were seeded on fibronectin-coated coverslips and stained for actin using rhodamine phalloidin. Yellow lines indicate the cross-section from which stress fibers were quantified (D) for number and width using ImageJ software. Data are means ± SD from a representative of two experiments in which ≥15 cells in 10 fields were counted for each condition. **P* = 0.03, *t* test. Scale bar, 10 μm. (**E** and **F**). Cell-cell junctions (arrows) of MDA-MB-231 cells transfected with a control or GFP-MTSS1 expression plasmid and seeded on fibronectin-coated slides, such that each cell touched its neighbors (E). (F) Data are representative of two experiments. **P* < 0.0001, χ^2 test. Scale bars, 10 μm.

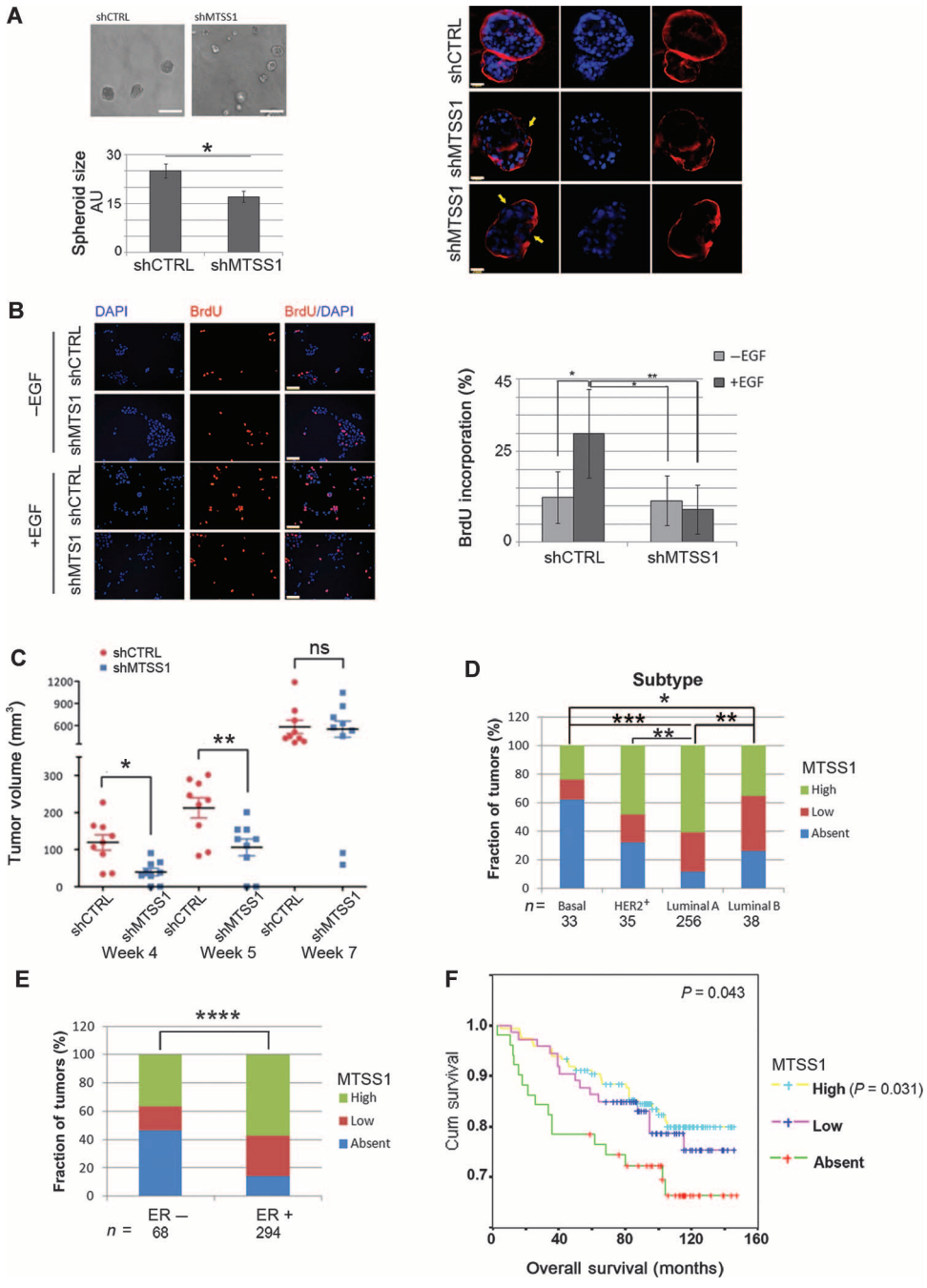

Fig. 7. Loss of MTSS1 suppresses the initial growth of mammary tumors but correlates with aggressive subtypes and poor patient prognosis. (**A**) Spheroid formation in Matrigel by control or MTSS1-depleted MCF10A cells. Left, representative phase images and quantification of spheroid size after 2 weeks; right, DAPI (4′,6-diamidino-2-phenylindole) (blue) and laminin 5 (red) staining of spheroids after 4 weeks. Arrows mark breaks in the encapsulating basement membrane. Data are means ± SD from two experiments. $^{*}P$ = 0.0006. AU, arbitrary units. Scale bars, 200 μm. (**B**) Proliferation assessed using BrdU incorporation by the indicated derivatives of MCF10A cells. Data are means ± SD from ≥8 non-overlapping photomicrograph fields, >500 nuclei each. $^{*}P$ = 0.001, $^{**}P$ = 0.00007, one-way ANOVA followed by Bonferroni correction. Scale bars, 100 μm. (**C**) Volume of orthotopic xenografts derived from MDA-MB-231 cells. Data are from nine mice per group. $^{*}P$ = 0.003, $^{**}P$ = 0.009, *t* test. ns, no statistical significance. The onset of tumors was also significantly delayed in shMTSS1 xenografts (P = 0.0031, χ^2 test). (**D** and **E**) MTSS1 abundance, classified as high (strong staining), low (weak staining), or absent (no staining), in breast tumor specimens grouped according to subtype (D) or ER status (E). Numbers below the bars correspond to the respective number of patients. $^{*}P$ = 0.013, $^{**}P$ = 0.011, $^{***}P = 4.03 \times 10^{-10}$, $^{****}P = 1.37 \times 10^{-7}$, χ^2 test. (**F**) Kaplan-Meier survival curves of deceased breast cancer patients stratified according to MTSS1 protein abundance. *P* values assessing the difference among the three curves (P = 0.043) or between that of patients with MTSS1-abundant tumors and those with MTSS1-absent tumors (P = 0.031) were calculated using the log-rank test. Data are from all patients (n = 362) assessed by immunohistochemistry (D).

that reducing MTSS1 abundance confers a growth disadvantage, in line with a role for MTSS1 in promoting proliferation at an early phase of growth in extracellular matrix.

To examine this hypothesis in vivo, we implanted MTSS1-depleted or control MDA-MB-231 cells into the mammary fat pad of immunocompromised female mice and monitored tumor size. Tumor onset was significantly delayed in mice implanted with MTSS1-depleted cells: 7 of the 10 control mice developed well-defined, palpable tumors by the end of the second week after implantation, but none of the nine mice injected with MTSS1-depleted cells did (Fig. 7C). Likewise, up until the end of the fifth week, tumor sizes were significantly different. However, by the end of the seventh week, tumors formed by both groups reached statistically indistinguishable sizes. These observations are reminiscent of results obtained using an MTSS1-overexpressing xenograft model of squamous carcinoma, which formed larger tumors at the initial phase, followed by comparable sizes later on (*43*). Together, these results attribute to MTSS1 a subtle growth-promoting role, which appears limited to the onset phase of tumor development and relates to the stimulatory effect of growth factors.

To evaluate potential clinical implications of MTSS1, we analyzed 362 breast cancer specimens, which we stratified using immunohistochemistry

according to MTSS1 abundance (fig. S5A). Similar to the analysis of mRNA abundance (Fig. 4B), MTSS1 protein abundance was significantly associated with molecular subtypes. For example, the relatively aggressive basal (Fig. 7D) and estrogen receptor (ER)–negative (Fig. 7E) subtypes had greater fractions of tumors with low or no detection of MTSS1 than highly abundant detection of MTSS1. Low or absent MTSS1 was also associated with higher tumor grades (fig. S5, B to D). In line with these observations, the shorter overall survival of patients of the cohort we analyzed was significantly associated with low or absent MTSS1 in the corresponding primary tumors (Fig. 7F). In conclusion, these results suggest that reduced abundance of MTSS1 correlates with an aggressive breast cancer phenotype and shorter survival time in patients.

DISCUSSION

Multiple newly synthesized RNA molecules underlie growth factor actions. These include not only mRNAs and a multitude of alternatively spliced forms (*44*, *45*) but also several types of noncoding RNAs. Using mammary cells that migrate in response to EGF, we previously identified the ID-miRs, a group of miRNAs that are rapidly suppressed in response to EGF (*7*). Using the same cell system, we grouped EGF-inducible miRNAs into two classes, IU-miRs and DU-miRs, and linked some of the IU-miRs to EGF-induced invasion phenotypes in mammary cells.

Large-scale miRNA data sets show aberrant abundance of specific miRNAs in tumors from breast cancer patients (*28, 29, 31*). Along this vein, we found that both the IU-miRs and DU-miRs were enriched among miRNAs that are differentially expressed in breast tumors. In addition, some IU-miRs were found to be associated with specific breast cancer molecular subtypes, implying that transcriptional processes instigated by a growth factor in a model system might bear relevance to pathogenesis. Indeed, we found that some IU-miRs, namely, let-7f, miR-15b, and miR-20a, are involved in migration and invasion of model mammary cells. The case of miR-15b is especially interesting: it was previously reported that depletion of miR-15b reduces proliferation and increases apoptosis of melanoma cells (*10*). Likewise, in cervical cancer, the abundance of miR-15b is increased and seems to promote invasion, metastasis, and angiogenesis (*46*). Nevertheless, miR-15b overexpression in a multidrug-resistant gastric cancer cell line induced apoptosis (*47*). In line with a dual role in tumor progression, expression of this miRNA might be enhanced by the E2F regulatory network (*48*, *49*), but it associates with repression of epithelial-mesenchymal transition in tongue cancer cells (*50*). Accordingly, miR-15b has several known targets, including *BCL2*, an antiapoptotic regulator, and *CCDN1*, a cell cycle promoter.

Here, we identified *MTSS1* as a direct target of miR-15b. The involvement of MTSS1 in cell proliferation and in tumor growth is complex [for a review, see (*51*)]. In general, the protein is overexpressed in primary tumors, but its abundance decreases in advanced lesions. However, it was found that ectopic MTSS1 induces a weak, but significant, decrease in cell proliferation in vitro, and the opposite effect was observed in MTSS1-depleted cells (*16*). On the contrary, we observed impaired 3D growth of MTSS1-depleted mammary cell cultures, as well as inhibited onset and slower initial growth of the respective xenografts in mice. These observations are similar to results obtained with a head and neck cancer model: overexpression of MTSS1 led to faster tumor growth, but later on, tumor cells showed less proliferation and more differentiation (*43*). In addition, depletion of MTSS1 in this model was accompanied by weaker signaling by the EGF receptor. Conceivably, MTSS1 is needed at an early phase for growth factor signaling, which regulates cell proliferation; at later stages, the migration-inhibiting functions of MTSS1 become more critical for tumor progression. Notably, it was found that MTSS1 positively modulates EGF signaling only at low cell densities (*43*). Confluence sensing might be mediated by cilia, which are MTSS1-controlled slender protuberances that project from the cell body (*40*). Whether ciliogenesis can explain the complex involvement and regulation of MTSS1 in tumor progression remains a matter for future research.

Because MTSS1 contains a combination of an I-BAR domain and a G-actin–binding motif, we focused our attention on membrane deformations that lead to cellular migration and endocytosis. Accordingly, we found that MTSS1 depletion increased motility of mammary cells, whereas ectopic MTSS1 expression reduced migration and invasion. These observations portray a complex role for MTSS1 in cellular motility: enhanced formation of invadopodia on the loss-of-function hand, and, on the other hand, diminution of actin stress fibers and formation of intercellular junctions. Although we were unable to elucidate the mechanism underlying the increase in invadopodia formation after MTSS1 knockdown, we speculate that it might relate to cortactin, an actin binder whose phosphorylation by the kinase Src is essential for invadopodia formation (*38*), but this is antagonized by MTSS1 (*40*). The loss of actin fibers is in agreement with previous reports, in which MTSS1 overexpression in sarcoma cells induced stress fiber loss (*42*), whereas diminished MTSS1 in mammary cells enhanced stress fibers through RhoA activation (*52*). Likewise, the observation that MTSS1 promotes intercellular junctions is supported by studies showing that MTSS1 is critical for kidney epithelia integrity (*25*) and for cell junction assembly (*24*).

Multiple mechanisms are responsible for MTSS1 decrease in cancer, including DNA methylation, proteasomal destruction (*53*), and post-transcriptional regulation by miR-23a (*20*), miR-182 (*19*), and miR-135a (*22*). This multiplicity might explain why the prognostic value of MTSS1 has remained an open issue (*51*). By using immunohistochemistry rather than RNA analysis, and by surveying a relatively large cohort of patients, we found that low abundance of the protein correlates with poor prognosis. These findings are consistent with studies that identified MTSS1 as a prognostic marker in gastric and breast cancer (*15*, *16*), and together with the induction of miR-15b by EGF, they uncover a new regulatory module involved in progression of aggressive breast tumors.

MATERIALS AND METHODS

Unless indicated, reagents and antibodies were purchased from Sigma-Aldrich. MCF10A cells were cultured in 2D and 3D (*54*) as previously described (*27*). The MDA-MB-231 and BT549 cell lines were grown in RPMI medium supplemented with 10% heat-inactivated fetal bovine serum, 1 mM sodium pyruvate, and a penicillin-streptomycin mixture.

All animal studies were approved by the Weizmann Institute's Institutional Review Board. CB-17 severe combined immunodeficient (SCID) female mice were maintained and treated under specific pathogen–free conditions. GFP-labeled cells (2×10^6 per mouse) were implanted in the fat pad of 5- to 6-week-old female mice. Eight weeks after implantation, mice were anesthetized and tumor size was measured. Statistical significance was examined with the two-sided Fisher's exact test or the Student's *t* test, as appropriate.

Total RNA was extracted using the miRNeasy Mini Kit (Qiagen). For mRNA expression, total RNA was isolated using PerfectPure RNA Cultured Cell Kit (5 PRIME). Complementary DNA was synthesized using the miScript Kit (Qiagen). Primers for miRNAs were designed according to the mature miRNA sequence (miRBase, Sanger Institute release 19, www.mirbase.org/index.shtml). Real-time qPCR analysis was performed with SYBR Green

(Qiagen or Applied Biosystems) and specific primers (see table S2). qPCR signals (C_T) were normalized to U6 small nuclear RNA or to *GAPDH* and B2M (β_2-microglobulin).

All anti-miR inhibitors and mimic miRNAs were purchased from Qiagen. All siRNAs were from Thermo Scientific Dharmacon (ON-TARGETplus). Transfections were performed using DharmaFECT 1 (Dharmacon) or Oligofectamine (Invitrogen Life Technologies). The full-length MTSS1-GFP plasmid was a gift from A. E. Oro (*42*). Transient plasmid transfections were performed using FuGENE HD (Promega) or Lipofectamine 2000 (Invitrogen Life Technologies). MTSS1-GFP, Control-GFP, and LifeAct-RFP sequences were cloned into a lentiviral construct using the pENTR Directional TOPO cloning kit (Invitrogen Life Technologies). Control and MTSS1 shRNA lentiviral particles (antisense sequence: 5′-ATGTCAGTTACATAGGTTG-3′) were obtained from Thermo Scientific. All analyses of the transiently transfected cells were done 72 hours after transfection.

For migration assays, we used previously described protocols (*27*). For invasion assays, cells were plated in the upper compartment of a Matrigel-coated membrane (BD Biosciences) and incubated for 20 to 22 hours at 37°C. The membranes were fixed in 3% paraformaldehyde, permeabilized in 0.5% Triton X-100, and stained with 0.3% methyl violet. Cells remaining on the upper side of the membrane were scraped, and cells that invaded to the bottom side of the membrane were photographed and then disintegrated for quantification in 0.1 N NaOH lysis solution containing SDS (1%).

Plasmids containing the 3′UTR of MTSS1 and a positive control were purchased from SwitchGear Genomics. The three-nucleotide mutation in the miR-15b seed was introduced using PCR, and the inserted mutation was confirmed by sequencing. For 3′UTR reporter assays, HeLa cells were co-transfected with a *Renilla* luciferase plasmid containing MTSS1, either a wild-type MTSS1-3′UTR, a MTSS1-3′UTR that carries a mutation in the sequence corresponding to the seed sequence of miR-15b, or a positive control 3′UTR, along with an anti–miR-15b or a control, nontargeting anti-miR. Additionally, the pGL3-Control vector containing firefly luciferase (Promega) was transfected as a control for transfection efficiency. Forty-eight hours after transfection, cells were harvested and firefly and *Renilla* luciferase activities were assayed with a dual-luciferase assay system (Promega) on the Modulus Microplate Reader. *Renilla* luciferase luminescence values were normalized to firefly luminescence and quantified relative to control.

Cells were plated on glass coverslips that were coated with fibronectin and fixed in 3% paraformaldehyde, followed by permeabilization in 0.2% Triton X-100 and blocking with 1% albumin. Thereafter, cells were incubated with the indicated primary antibody and labeled with a fluorescent secondary antibody. Live-cell imaging and immunofluorescence of fixed cells were performed using a DeltaVision microscope (Applied Precision).

Cells were scraped in solubilization buffer [50 mM Hepes (pH 7.5), 150 mM NaCl, 10% glycerol, 1% Triton X-100, 1 mM EDTA, 1 mM EGTA, 10 mM NaF, 30 mM β-glycerol phosphate, 0.2 mM Na_3VO_4, and a protease inhibitor cocktail]. Boiled lysates were separated using SDS–polyacrylamide gel electrophoresis and transferred using electrophoresis to a nitrocellulose membrane. After transfer, nitrocellulose membranes were blocked in TBST buffer [0.02 M tris-HCl (pH 7.5), 0.15 M NaCl, and 0.05% Tween 20] containing 5% low-fat milk and incubated for 16 hours with the indicated primary antibody. Thereafter, blots were washed in TBST (tris-buffered saline–Tween 20) and incubated for 30 min with a secondary antibody linked to horseradish peroxidase.

Glass coverslips were inverted on a drop containing both unlabeled gelatin and Alexa Fluor 488–gelatin (Molecular Probes) at an 8:1 ratio. Cells (4×10^4/ml) were plated on the gelatin-coated coverslips in a 24-well plate, incubated at 37°C for 4 hours, and fixed in 3% paraformaldehyde. After fixation, cells were stained with rhodamine phalloidin.

Formalin-fixed, paraffin-embedded breast tumors were analyzed using the EnVision Detection System (DakoCytomation). Antigen retrieval was performed with an ethylenediaminetetraacetic solution (pH 9.0) at 98°C for 20 min. The MTSS1 antibody was incubated overnight at 4°C. Two pathologists independently assessed protein levels and scored them based on staining intensity. Statistical analysis of the data was done using the SPSS suite.

Cell were incubated with the BrdU labeling reagent for 3 hours, and then fixed and stained using a BrdU detection kit (Roche Diagnostics GmbH). Visualization of the cells was done using a Nikon Eclipse 90i microscope, and photos were captured using the Image-Pro software. BrdU- and DAPI-stained nuclei were counted from at least 15 fields of each treatment.

Predictions of potential targets for specific miRNAs were found using the miRecords resource (*33*) (http://mirecords.biolead.org/), which integrates the prediction results from 11 different prediction tools. Only targets that were predicted by at least five different tools were selected. Further filtering of the targets was done by crossing the list of predicted targets with lists of transcripts, the abundance of which was suppressed after treatment of cells with EGF (*6*).

A breast cancer miRNA expression data set (*28*) was analyzed using Sorting Points Into Neighborhood (SPIN). SPIN is an unsupervised method for sorting and visualization of multidimensional data (*55*). Statistically significant differences were calculated using Student's *t* test, one- or two-way ANOVA, and χ^2 test, as appropriate.

SUPPLEMENTARY MATERIALS

Fig. S1. Validation of miRNA induction upon stimulation with EGF.
Fig. S2. Specific DU-miRs inhibit cell migration when ectopically expressed.
Fig. S3. Knockdown of MTSS1 depletes several isoforms, increases cell motility, and augments formation of invadopodia in breast cancer cells.
Fig. S4. MTSS1- and miR-15b–manipulated cells show altered motility.
Fig. S5. MTSS1 abundance is associated with breast cancer markers.
Table S1. *P* and *q* values of IU-miRs associated with breast cancer subtypes.
Table S2. qRT-PCR primer sequences.

REFERENCES AND NOTES

1. N. E. Hynes, C. J. Watson, Mammary gland growth factors: Roles in normal development and in cancer. *Cold Spring Harb. Perspect. Biol.* **2**, a003186 (2010).
2. E. Witsch, M. Sela, Y. Yarden, Roles for growth factors in cancer progression. *Physiology* **25**, 85–101 (2010).

3. M. Katz, I. Amit, A. Citri, T. Shay, S. Carvalho, S. Lavi, F. Milanezi, L. Lyass, N. Amariglio, J. Jacob-Hirsch, N. Ben-Chetrit, G. Tarcic, M. Lindzen, R. Avraham, Y. C. Liao, P. Trusk, A. Lyass, G. Rechavi, N. L. Spector, S. H. Lo, F. Schmitt, S. S. Bacus, Y. Yarden, A reciprocal tensin-3–cten switch mediates EGF-driven mammary cell migration. *Nat. Cell Biol.* **9**, 961–969 (2007).
4. H. D. Kim, T. W. Guo, A. P. Wu, A. Wells, F. B. Gertler, D. A. Lauffenburger, Epidermal growth factor–induced enhancement of glioblastoma cell migration in 3D arises from an intrinsic increase in speed but an extrinsic matrix- and proteolysis-dependent increase in persistence. *Mol. Biol. Cell* **19**, 4249–4259 (2008).
5. A. Albasri, M. Aleskandarany, A. Benhasouna, D. G. Powe, I. O. Ellis, M. Ilyas, A. R. Green, CTEN (C-terminal tensin-like), a novel oncogene overexpressed in invasive breast carcinoma of poor prognosis. *Breast Cancer Res. Treat.* **126**, 47–54 (2011).
6. I. Amit, A. Citri, T. Shay, Y. Lu, M. Katz, F. Zhang, G. Tarcic, D. Siwak, J. Lahad, J. Jacob-Hirsch, N. Amariglio, N. Vaisman, E. Segal, G. Rechavi, U. Alon, G. B. Mills, E. Domany, Y. Yarden, A module of negative feedback regulators defines growth factor signaling. *Nat. Genet.* **39**, 503–512 (2007).
7. R. Avraham, A. Sas-Chen, O. Manor, I. Steinfeld, R. Shalgi, G. Tarcic, N. Bossel, A. Zeisel, I. Amit, Y. Zwang, E. Enerly, H. G. Russnes, F. Biagioni, M. Mottolese, S. Strano, G. Blandino, A. L. Borresen-Dale, Y. Pilpel, Z. Yakhini, E. Segal, Y. Yarden, EGF decreases the abundance of microRNAs that restrain oncogenic transcription factors. *Sci. Signal.* **3**, ra43 (2010).
8. R. Avraham, Y. Yarden, Feedback regulation of EGFR signalling: Decision making by early and delayed loops. *Nat. Rev. Mol. Cell Biol.* **12**, 104–117 (2011).
9. L. Lin, Y. Lin, Y. Jin, C. Zheng, Microarray analysis of microRNA expression in liver cancer tissues and normal control. *Gene* **523**, 158–160 (2013).
10. I. Satzger, A. Mattern, U. Kuettler, D. Weinspach, B. Voelker, A. Kapp, R. Gutzmer, MicroRNA-15b represents an independent prognostic parameter and is correlated with tumor cell proliferation and apoptosis in malignant melanoma. *Int. J. Cancer* **126**, 2553–2562 (2010).
11. X. Wang, S. Tang, S. Y. Le, R. Lu, J. S. Rader, C. Meyers, Z. M. Zheng, Aberrant expression of oncogenic and tumor-suppressive microRNAs in cervical cancer is required for cancer cell growth. *PLOS One* **3**, e2557 (2008).
12. Y. Xi, A. Formentini, M. Chien, D. B. Weir, J. J. Russo, J. Ju, M. Kornmann, J. Ju, Prognostic values of microRNAs in colorectal cancer. *Biomark. Insights* **2**, 113–121 (2006).
13. H. Xia, Y. Qi, S. S. Ng, X. Chen, S. Chen, M. Fang, D. Li, Y. Zhao, R. Ge, G. Li, Y. Chen, M. L. He, H. F. Kung, L. Lai, M. C. Lin, MicroRNA-15b regulates cell cycle progression by targeting cyclins in glioma cells. *Biochem. Biophys. Res. Commun.* **380**, 205–210 (2009).
14. Y. G. Lee, J. A. Macoska, S. Korenchuk, K. J. Pienta, MIM, a potential metastasis suppressor gene in bladder cancer. *Neoplasia* **4**, 291–294 (2002).
15. K. Liu, G. Wang, H. Ding, Y. Chen, G. Yu, J. Wang, Downregulation of metastasis suppressor 1(MTSS1) is associated with nodal metastasis and poor outcome in Chinese patients with gastric cancer. *BMC Cancer* **10**, 428 (2010).
16. C. Parr, W. G. Jiang, Metastasis suppressor 1 (MTSS1) demonstrates prognostic value and anti-metastatic properties in breast cancer. *Eur. J. Cancer* **45**, 1673–1683 (2009).
17. H. Hirata, K. Ueno, V. Shahryari, G. Deng, Y. Tanaka, Z. L. Tabatabai, Y. Hinoda, R. Dahiya, MicroRNA-182-5p promotes cell invasion and proliferation by down regulating *FOXF2*, *RECK* and *MTSS1* genes in human prostate cancer. *PLOS One* **8**, e55502 (2013).
18. Z. Liu, J. Liu, M. F. Segura, C. Shao, P. Lee, Y. Gong, E. Hernando, J. J. Wei, *MiR-182* overexpression in tumourigenesis of high-grade serous ovarian carcinoma. *J. Pathol.* **228**, 204–215 (2012).
19. J. Wang, J. Li, J. Shen, C. Wang, L. Yang, X. Zhang, MicroRNA-182 downregulates metastasis suppressor 1 and contributes to metastasis of hepatocellular carcinoma. *BMC Cancer* **12**, 227 (2012).
20. S. Jahid, J. Sun, R. A. Edwards, D. Dizon, N. C. Panarelli, J. W. Milsom, S. S. Sikandar, Z. H. Gümüs, S. M. Lipkin, miR-23a promotes the transition from indolent to invasive colorectal cancer. *Cancer Discov.* **2**, 540–553 (2012).
21. S. Liu, W. Guo, J. Shi, N. Li, X. Yu, J. Xue, X. Fu, K. Chu, C. Lu, J. Zhao, D. Xie, M. Wu, S. Cheng, S. Liu, MicroRNA-135a contributes to the development of portal vein tumor thrombus by promoting metastasis in hepatocellular carcinoma. *J. Hepatol.* **56**, 389–396 (2012).
22. W. Zhou, X. Li, F. Liu, Z. Xiao, M. He, S. Shen, S. Liu, MiR-135a promotes growth and invasion of colorectal cancer via metastasis suppressor 1 in vitro. *Acta Biochim. Biophys. Sin.* **44**, 838–846 (2012).
23. P. K. Mattila, A. Pykäläinen, J. Saarikangas, V. O. Paavilainen, H. Vihinen, E. Jokitalo, P. Lappalainen, Missing-in-metastasis and IRSp53 deform PI(4,5)P_2-rich membranes by an inverse BAR domain–like mechanism. *J. Cell Biol.* **176**, 953–964 (2007).
24. J. C. Dawson, S. Bruche, H. J. Spence, V. M. Braga, L. M. Machesky, Mtss1 promotes cell-cell junction assembly and stability through the small GTPase Rac1. *PLOS One* **7**, e31141 (2012).
25. J. Saarikangas, P. K. Mattila, M. Varjosalo, M. Bovellan, J. Hakanen, J. Calzada-Wack, M. Tost, L. Jennen, B. Rathkolb, W. Hans, M. Horsch, M. E. Hyvönen, N. Perälä, H. Fuchs, V. Gailus-Durner, I. Esposito, E. Wolf, M. H. de Angelis, M. J. Frilander, H. Savilahti, H. Sariola, K. Sainio, S. Lehtonen, J. Taipale, M. Salminen, P. Lappalainen, Missing-in-metastasis MIM/MTSS1 promotes actin assembly at intercellular junctions and is required for integrity of kidney epithelia. *J. Cell Sci.* **124**, 1245–1255 (2011).
26. S. E. Seton-Rogers, Y. Lu, L. M. Hines, M. Koundinya, J. LaBaer, S. K. Muthuswamy, J. S. Brugge, Cooperation of the ErbB2 receptor and transforming growth factor β in induction of migration and invasion in mammary epithelial cells. *Proc. Natl. Acad. Sci. U.S.A.* **101**, 1257–1262 (2004).
27. G. Tarcic, R. Avraham, G. Pines, I. Amit, T. Shay, Y. Lu, Y. Zwang, M. Katz, N. Ben-Chetrit, J. Jacob-Hirsch, L. Virgilio, G. Rechavi, G. Mavrothalassitis, G. B. Mills, E. Domany, Y. Yarden, EGR1 and the ERK-ERF axis drive mammary cell migration in response to EGF. *FASEB J.* **26**, 1582–1592 (2012).
28. F. Biagioni, N. Bossel Ben-Moshe, G. Fontemaggi, V. Canu, F. Mori, B. Antoniani, A. Di Benedetto, R. Santoro, S. Germoni, F. De Angelis, A. Cambria, R. Avraham, G. Grasso, S. Strano, P. Muti, M. Mottolese, Y. Yarden, E. Domany, G. Blandino, miR-10b*, a master inhibitor of the cell cycle, is down-regulated in human breast tumours. *EMBO Mol. Med.* **4**, 1214–1229 (2012).
29. E. Enerly, I. Steinfeld, K. Kleivi, S. K. Leivonen, M. R. Aure, H. G. Russnes, J. A. Rønneberg, H. Johnsen, R. Navon, E. Rødland, R. Mäkelä, B. Naume, M. Perälä, O. Kallioniemi, V. N. Kristensen, Z. Yakhini, A. L. Børresen-Dale, miRNA-mRNA integrated analysis reveals roles for miRNAs in primary breast tumors. *PLOS One* **6**, e16915 (2011).
30. C. Blenkiron, L. D. Goldstein, N. P. Thorne, I. Spiteri, S. F. Chin, M. J. Dunning, N. L. Barbosa-Morais, A. E. Teschendorff, A. R. Green, I. O. Ellis, S. Tavaré, C. Caldas, E. A. Miska, MicroRNA expression profiling of human breast cancer identifies new markers of tumor subtype. *Genome Biol.* **8**, R214 (2007).
31. H. Dvinge, A. Git, S. Gräf, M. Salmon-Divon, C. Curtis, A. Sottoriva, Y. Zhao, M. Hirst, J. Armisen, E. A. Miska, S. F. Chin, E. Provenzano, G. Turashvili, A. Green, I. Ellis, S. Aparicio, C. Caldas, The shaping and functional consequences of the microRNA landscape in breast cancer. *Nature* **497**, 378–382 (2013).
32. N. Bossel Ben-Moshe, R. Avraham, M. Kedmi, A. Zeisel, A. Yitzhaky, Y. Yarden, E. Domany, Context-specific microRNA analysis: Identification of functional microRNAs and their mRNA targets. *Nucleic Acids Res.* **40**, 10614–10627 (2012).
33. F. Xiao, Z. Zuo, G. Cai, S. Kang, X. Gao, T. Li, miRecords: An integrated resource for microRNA–target interactions. *Nucleic Acids Res.* **37**, D105–D110 (2009).
34. G. R. White, J. M. Varley, J. Heighway, Isolation and characterization of a human homologue of the latrophilin gene from a region of 1p31.1 implicated in breast cancer. *Oncogene* **17**, 3513–3519 (1998).
35. L. M. Machesky, S. A. Johnston, MIM: A multifunctional scaffold protein. *J. Mol. Med.* **85**, 569–576 (2007).
36. R. D. Loberg, C. K. Neeley, L. L. Adam-Day, Y. Fridman, L. N. St. John, S. Nixdorf, P. Jackson, L. M. Kalikin, K. J. Pienta, Differential expression analysis of MIM (MTSS1) splice variants and a functional role of MIM in prostate cancer cell biology. *Int. J. Oncol.* **26**, 1699–1705 (2005).
37. J. Lin, J. Liu, Y. Wang, J. Zhu, K. Zhou, N. Smith, X. Zhan, Differential regulation of cortactin and N-WASP-mediated actin polymerization by missing in metastasis (MIM) protein. *Oncogene* **24**, 2059–2066 (2005).
38. D. A. Murphy, S. A. Courtneidge, The 'ins' and 'outs' of podosomes and invadopodia: Characteristics, formation and function. *Nat. Rev. Mol. Cell Biol.* **12**, 413–426 (2011).
39. K. L. Burger, B. S. Learman, A. K. Boucherle, S. J. Sirintrapun, S. Isom, B. Diaz, S. A. Courtneidge, D. F. Seals, Src-dependent Tks5 phosphorylation regulates invadopodia-associated invasion in prostate cancer cells. *Prostate* **74**, 134–148 (2014).
40. M. Bershteyn, S. X. Atwood, W. M. Woo, M. Li, A. E. Oro, MIM and cortactin antagonism regulates ciliogenesis and hedgehog signaling. *Dev. Cell* **19**, 270–283 (2010).
41. P. K. Mattila, M. Salminen, T. Yamashiro, P. Lappalainen, Mouse MIM, a tissue-specific regulator of cytoskeletal dynamics, interacts with ATP-actin monomers through its C-terminal WH2 domain. *J. Biol. Chem.* **278**, 8452–8459 (2003).
42. R. Gonzalez-Quevedo, M. Shoffer, L. Horng, A. E. Oro, Receptor tyrosine phosphatase–dependent cytoskeletal remodeling by the hedgehog-responsive gene *MIM/BEG4*. *J. Cell Biol.* **168**, 453–463 (2005).
43. J. C. Dawson, P. Timpson, G. Kalna, L. M. Machesky, Mtss1 regulates epidermal growth factor signaling in head and neck squamous carcinoma cells. *Oncogene* **31**, 1781–1793 (2012).
44. W. J. Köstler, A. Zeisel, C. Körner, J. M. Tsai, J. Jacob-Hirsch, N. Ben-Chetrit, K. Sharma, H. Cohen-Dvashi, A. Yitzhaky, E. Lader, U. Tschulena, G. Rechavi, E. Domany, S. Wiemann, Y. Yarden, Epidermal growth-factor–induced transcript isoform variation drives mammary cell migration. *PLOS One* **8**, e80566 (2013).
45. A. Zeisel, W. J. Köstler, N. Molotski, J. M. Tsai, R. Krauthgamer, J. Jacob-Hirsch, G. Rechavi, Y. Soen, S. Jung, Y. Yarden, E. Domany, Coupled pre-mRNA and mRNA dynamics unveil operational strategies underlying transcriptional responses to stimuli. *Mol. Syst. Biol.* **7**, 529 (2011).
46. Y. Gómez-Gómez, J. Organista-Nava, P. Gariglio, Deregulation of the miRNAs expression in cervical cancer: Human papillomavirus implications. *Biomed Res. Int.* **2013**, 407052 (2013).

47. L. Xia, D. Zhang, R. Du, Y. Pan, L. Zhao, S. Sun, L. Hong, J. Liu, D. Fan, miR-15b and miR-16 modulate multidrug resistance by targeting BCL2 in human gastric cancer cells. *Int. J. Cancer* **123**, 372–379 (2008).
48. M. P. Myklebust, O. Bruland, O. Fluge, A. Skarstein, L. Balteskard, O. Dahl, MicroRNA-15b is induced with E2F-controlled genes in HPV-related cancer. *Br. J. Cancer* **105**, 1719–1725 (2011).
49. M. Ofir, D. Hacohen, D. Ginsberg, MiR-15 and miR-16 are direct transcriptional targets of E2F1 that limit E2F-induced proliferation by targeting cyclin E. *Mol. Cancer Res.* **9**, 440–447 (2011).
50. L. Sun, Y. Yao, B. Liu, Z. Lin, L. Lin, M. Yang, W. Zhang, W. Chen, C. Pan, Q. Liu, E. Song, J. Li, MiR-200b and miR-15b regulate chemotherapy-induced epithelial-mesenchymal transition in human tongue cancer cells by targeting BMI1. *Oncogene* **31**, 432–445 (2012).
51. F. Xie, L. Ye, M. Ta, L. Zhang, W. G. Jiang, MTSS1: A multifunctional protein and its role in cancer invasion and metastasis. *Front. Biosci. (Schol. Ed.)* **3**, 621–631 (2011).
52. R. Lei, J. Tang, X. Zhuang, R. Deng, G. Li, J. Yu, Y. Liang, J. Xiao, H. Y. Wang, Q. Yang, G. Hu, Suppression of MIM by microRNA-182 activates RhoA and promotes breast cancer metastasis. *Oncogene* **33**, 1287–1296 (2014).
53. J. Zhong, S. Shaik, L. Wan, A. E. Tron, Z. Wang, L. Sun, H. Inuzuka, W. Wei, $SCF^{\beta\text{-}TRCP}$ targets MTSS1 for ubiquitination-mediated destruction to regulate cancer cell proliferation and migration. *Oncotarget* **4**, 2339–2353 (2013).
54. C. R. Pradeep, W. J. Köstler, M. Lauriola, R. Z. Granit, F. Zhang, J. Jacob-Hirsch, G. Rechavi, H. B. Nair, B. T. Hennessy, A. M. Gonzalez-Angulo, R. R. Tekmal, I. Ben-Porath, G. B. Mills, E. Domany, Y. Yarden, Modeling ductal carcinoma in situ: A HER2-Notch3 collaboration enables luminal filling. *Oncogene* **31**, 907–917 (2012).
55. D. Tsafrir, I. Tsafrir, L. Ein-Dor, O. Zuk, D. A. Notterman, E. Domany, Sorting points into neighborhoods (SPIN): Data analysis and visualization by ordering distance matrices. *Bioinformatics* **21**, 2301–2308 (2005).

Acknowledgments: This work was performed at the Marvin Tanner Laboratory for Cancer Research. We thank A. Oro and R. Avraham for plasmids and help. **Funding:** Our research is supported by the National Cancer Institute, the European Research Council, the Seventh Framework Program of the European Commission, the German-Israeli Project Cooperation (DIP), the Israel Cancer Research Fund, and the Dr. Miriam and Sheldon G. Adelson Medical Research Foundation. Y.Y. is the incumbent of the Harold and Zelda Goldenberg Professorial Chair. **Author contributions:** M.K., N.B.-C., C.K., M.M., N.B.B.-M., M.L., S.L., F.B., S.C., and H.C.-D. performed experiments or analyzed the data. F.S., S.W., and G.B. supervised specific analyses. M.K. and Y.Y. designed experiments and analyzed the data. M.K. and Y.Y. conceived the study and wrote the manuscript. **Competing interests:** The authors declare that they have no competing interests. **Data and materials availability:** Requests for reagents should be directed to Y.Y. Microarray data were obtained from GEO series GSE19536 (*29*).